Applied Catalysis B: Environmental 198 (2016) 162–170

Contents lists available at ScienceDirect

Applied Catalysis B: Environmental

journal homepage: www.elsevier.com/locate/apcatb

Ceria supported rhodium nanoparticles: Superb catalytic activity in hydrogen generation from the hydrolysis of ammonia borane

Serdar Akbayrak[a], Yalçın Tonbul[a,b], Saim Özkar[a,*]

[a] Department of Chemistry, Middle East Technical University, 06800 Ankara, Turkey
[b] Ziya Gökalp Faculty of Education, Dicle University, 21280 Diyarbakır, Turkey

ARTICLE INFO

Article history:
Received 12 April 2016
Received in revised form 21 May 2016
Accepted 24 May 2016
Available online 24 May 2016

Keywords:
Ceria
Rhodium nanoparticles
Ammonia borane
Hydrogen generation
Catalytic hydrolysis

ABSTRACT

We investigated the effect of various oxide supports on the catalytic activity of rhodium nanoparticles in hydrogen generation from the hydrolysis of ammonia borane. Among the oxide supports (CeO_2, SiO_2, Al_2O_3, TiO_2, ZrO_2, HfO_2) ceria provides the highest catalytic activity for the rhodium(0) nanoparticles in the hydrolysis of ammonia borane. Rhodium(0) nanoparticles supported on nanoceria (Rh^0/CeO_2) were prepared by the impregnation of rhodium(III) ions on the surface of ceria followed by their reduction with sodium borohydride in aqueous solution at room temperature. They were isolated from the reaction solution by centrifugation and characterized by a combination of advanced analytical techniques. The catalytic activity of Rh^0/CeO_2 samples with various rhodium loading in the range of 0.1–4.0% wt. Rh was also tested in hydrogen generation from the hydrolysis of ammonia borane at room temperature. The highest catalytic activity was achieved by using 0.1% wt. rhodium loaded nanoceria. The resulting Rh^0/CeO_2 with a metal loading of 0.1% wt. Rh show superb catalytic activity in hydrogen generation from the hydrolysis of ammonia borane with a record turnover frequency value (TOF) of 2010 min^{-1} at 25.0 ± 0.1 °C. The superb catalytic activity of Rh^0/CeO_2 is ascribed to the reducible nature of ceria. The reduction of cerium(IV) to cerium(III) leads to a build-up of negative charge on the oxide surface which favors the bonding of rhodium(0) nanoparticles on the surface and, thus, their catalytic activity. Rh^0/CeO_2 are also reusable catalysts preserving 67% of their initial catalytic activity even after the fifth use in hydrogen generation from the hydrolysis of ammonia borane at room temperature (TOF = 1350 min^{-1}. The work reported here also includes the kinetic studies depending on the temperature to determine the activation energy (E_a = 43 ± 2 kJ/mol) and the effect of catalyst concentration on the rate of hydrolysis of ammonia borane.

1. Introduction

Ammonia borane (NH_3BH_3, AB) is one of the most promising solid hydrogen storage materials for on-board hydrogen applications due to its high hydrogen storage capacity (19.6% wt.), non-toxicity, and high stability under ambient conditions [1–6]. Ammonia borane can release 3 equivalent H_2 upon hydrolysis in the presence of suitable catalysts even at ambient temperature according to Eq. (1).

$$H_3NBH_3(aq) + 2H_2O(l) \overset{catalyst}{\rightarrow} NH_4^+(aq) + BO_2^-(aq) + 3H_2(g)$$

Although a large variety of catalysts including noble [7–10] and non-noble [11–14] metal nanoparticles have been tested in hydrogen generation from the hydrolysis of ammonia borane, the development of efficient and stable catalysts is still an important challenge in using ammonia borane as solid hydrogen storage materials for the fuel cell applications under moderate conditions [15]. So far rhodium(0) nanoparticles supported on carbon nanotubes have been reported to be the highest activity catalyst with a turnover frequency of 706 min^{-1} in hydrogen generation from the hydrolysis of ammonia borane at room temperature [16]. Therefore it is quite plausible to give effort for further improving the catalytic activity of rhodium nanoparticles in this industrially important reaction. The catalytic performance of metal nanoparticles depends on the particle size and dispersion of the active sites while the reusability and catalytic lifetime of nanoparticles are affected by their stability against agglomeration [17]. Stable metal nanoparticles catalysts can be obtained by using suitable stabilizer ligands or supporting materials with large surface area [18–20]. Recent studies have shown that metal nanoparticles supported on reducible

* Corresponding author.
E-mail address: sozkar@metu.edu.tr (S. Özkar).

http://dx.doi.org/10.1016/j.apcatb.2016.05.061
0926-3373/

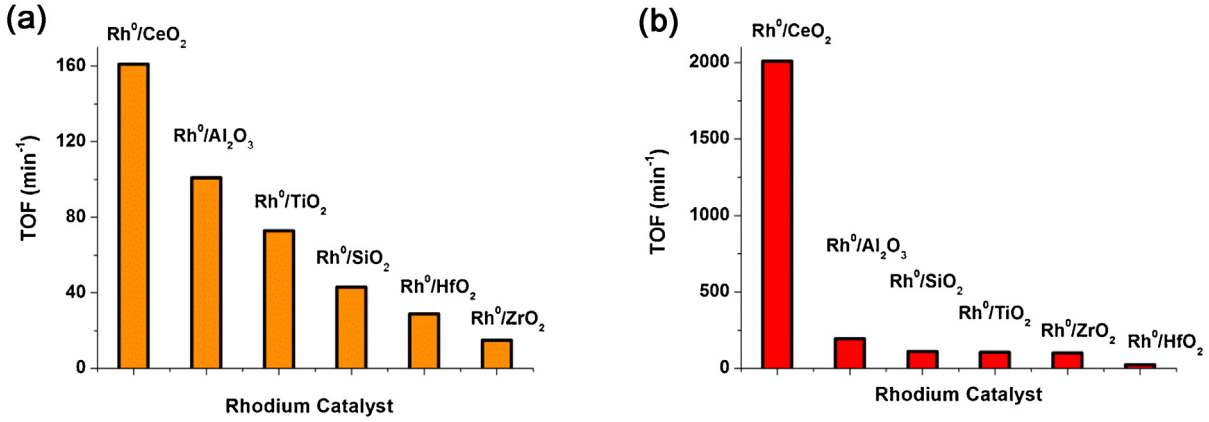

Fig. 1. Comparison of TOF (turnover frequency in mol H_2/(mol Rh × min)) values of rhodium nanoparticles supported on different oxides at (a) high and (b) low rhodium loadings of catalysts used in hydrogen generation from the hydrolysis of ammonia borane (10 mL,100 mM) at 25.0 ± 0.1 °C. For all the tests Rh/AB molar ratio of 0.0008 was used and no correction has been made for the initial TOF values by the fraction of catalytically active surface sites.

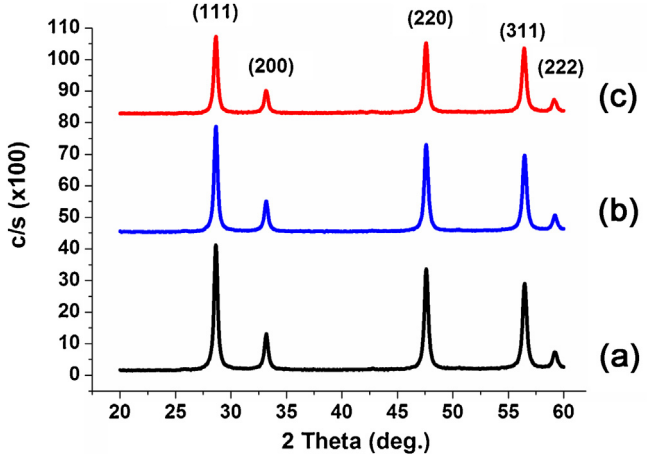

Fig. 2. Powder XRD patterns of (a) CeO_2, (b) Rh^0/CeO_2 with a 0.1% wt. Rh loading, (c) Rh^{00}/CeO_2 with a 3.42% wt. Rh loading.

oxides such as ceria (CeO_2) provide high catalytic activity in many reactions [21]. Cerium oxides have cerium(III) defects which can readily be formed because of the favorable large positive standard reduction potential of $Ce^{4+} \rightarrow Ce^{3+}$ (1.76 V in acidic solution [22]). It is conceivable that the interconversion of two oxidation states cerium(IV) and cerium(III) can occur under the catalytic reaction conditions, that is, ceria can undergo redox cycling in aqueous solution [23]. The formation of cerium(III) causes an excess negative charge to build up on the oxide surface which enhances the coordination of metal(0) nanoparticles to the oxide surface and, thus, the catalytic activity through a more favorable substrate-metal interaction [24]. Therefore, ceria has been used to improve the catalytic performance of transition metals through strong metal–support interaction, in particular, of the electron rich late-transition metal nanoparticles [25–27]. Although the mechanism of the promoting effect of cerium oxides has not been well understood yet, ceria has found broad applications in the field of catalysis such as in water splitting reactions [28,29], water–gas shift reactions [30,31], hydrogen generation from ammonia borane [32], decomposition of hydrazine [33], methanol synthesis from carbon dioxide [34], removal of nitrogen oxides from exhaust gases [35,36], and formic acid oxidation [37].

Herein we report the preparation, characterization, and catalytic use of rhodium(0) nanoparticles supported on nanoceria, Rh^0/CeO_2. For comparison, nanopowders of silica (SiO_2), alumina (Al_2O_3), titania (TiO_2), zirconia (ZrO_2), and hafnia (HfO_2) were also employed as support for the rhodium(0) nanoparticles catalyst in hydrolysis of ammonia borane under the same conditions. The comparative study shows that Rh^0/CeO_2 has superior catalytic activity with a turnover frequency of TOF = 2010 min^{-1} in hydrogen generation from the hydrolysis of ammonia borane at 25.0 ± 0.1 °C. Our report also shows that the nanoceria supported rhodium(0) nanoparticles are reusable catalyst providing a TOF value of 1350 min^{-1} after the fifth run of hydrogen generation from the complete hydrolysis of ammonia borane at 25.0 ± 0.1 °C.

2. Experimental

2.1. Materials

Rhodium(III) chloride hydrate ($RhCl_3{\cdot}3H_2O$), ammonia borane (AB, 97%), nanoceria (CeO_2, particle size ≈ 25 nm), nanotitania (TiO_2, particle size ≈ 25 nm), nanozirconia (ZrO_2, particle size ≈ 100 nm), hafnia (HfO_2, particle size ≈ 100 nm), nanoalumina (Al_2O_3, particle size ≈ 13 nm), and nanosilica (SiO_2, particle size ≈ 12 nm) were purchased from Aldrich. Deionized water was distilled by water purification system (Milli-QSystem). All glassware and Teflon-coated magnetic stir bars were cleaned with acetone, followed by copious rinsing with distilled water before drying in an oven at 150 °C.

2.2. Characterization

The rhodium content of Rh^0/CeO_2 samples was determined by the Inductively Coupled Plasma Optical Emission Spectroscopy (ICP-OES, Leeman-Direct Reading Echelle) after each sample was completely dissolved in the mixture of HNO_3/HCl (1/3 ratio). Transmission electron microscopy (TEM) was performed on a JEM-2100F (JEOL) microscope operating at 200 kV. Samples were examined at magnification between 400 K and 700 K. Scanning electron microscope (SEM) images were taken using a JEOL JSM-5310LVat 15 kV and 33 Pa in a low-vacuum mode without metal coating on aluminum support. The X-ray photoelectron spectroscopy (XPS) analysis was performed on a Physical Electronics 5800 spectrometer equipped with a hemispherical analyzer and using monochromatic Al Kα radiation of 1486.6 eV, the X-ray tube working at 15 kV, 350 W and pass energy of 23.5 keV. ^{11}B NMR spectra were recorded on a Bruker Avance DPX 400 with an operating frequency of 128.15 MHz for ^{11}B.

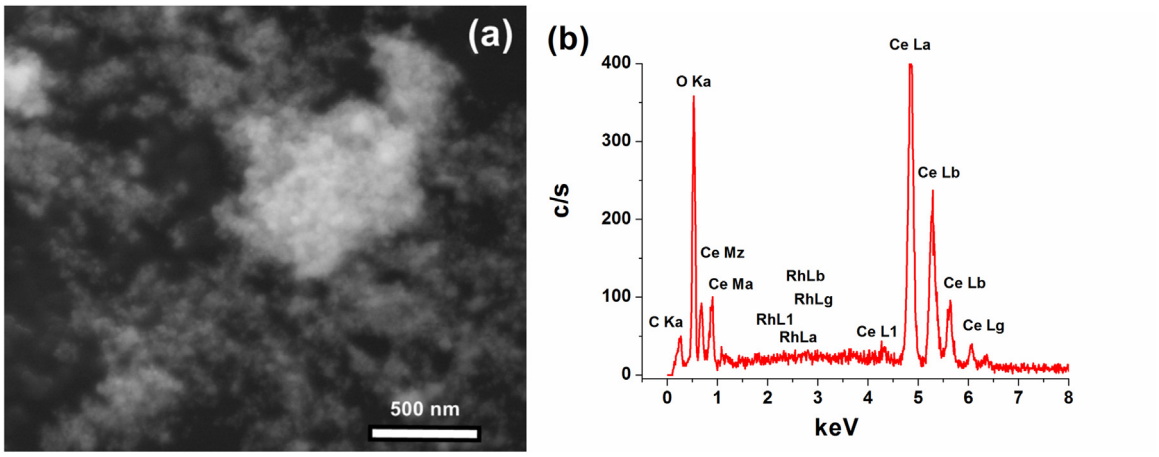

Fig. 3. (a) SEM image and (b) SEM-EDS spectrum of Rh^0/CeO_2 with a 0.1% wt. Rh loading.

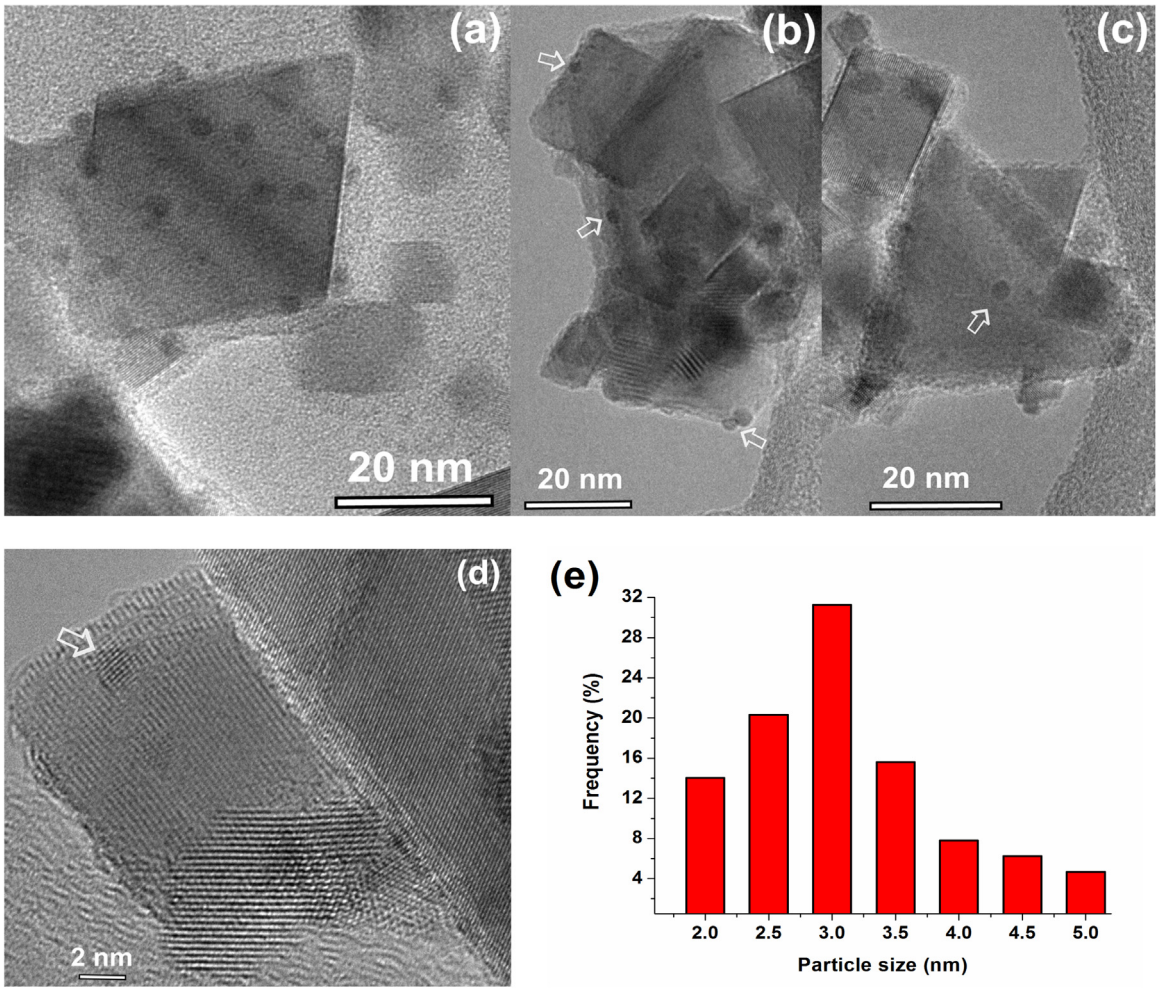

Fig. 4. TEM images of Rh^0/CeO_2 with a 0.1% wt. Rh loading at different magnifications (a–d) and the corresponding histogram showing the particle size distribution (e).

2.3. Preparation of rhodium(0) nanoparticles supported on ceria

Ceria (500 mg) was added to a solution of $RhCl_3{\cdot}3H_2O$ (in the amount required for the desired rhodium loading) in 100 mL H_2O in a 250 mL round bottom flask. This slurry was stirred at room temperature for 4 h and, then, 10 mL of 5 mM $NaBH_4$ solution was added dropwise. After 30 min stirring Rh^0/CeO_2 were formed which were isolated by centrifugation and washed with 100 mL of water. The remnant was dried under vacuum (10^{-3} torr) at 60 °C for 12 h. For comparison, Rh^0/SiO_2, Rh^0/Al_2O_3, Rh^0/TiO_2, Rh^0/ZrO_2, and Rh^0/HfO_2 were prepared by following the same procedure as described above, by using silica, alumina, titania, zirconia, or hafnia, respectively, instead of ceria.

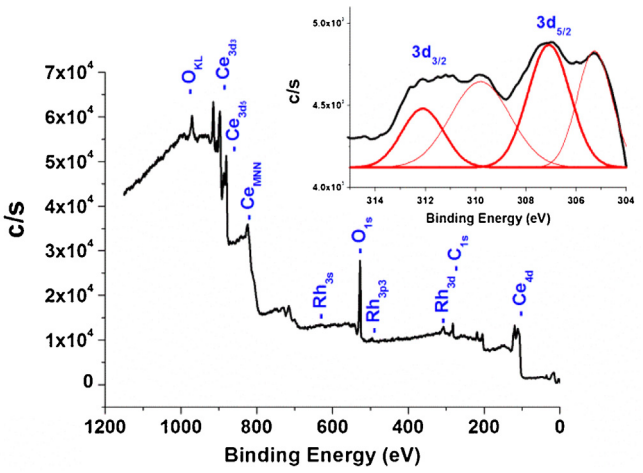

Fig. 5. X-ray photoelectron spectrum of Rh^0/CeO_2 with a 0.1% wt. Rh loading. The inset shows the high resolution scan and deconvolution of Rh 3d bands.

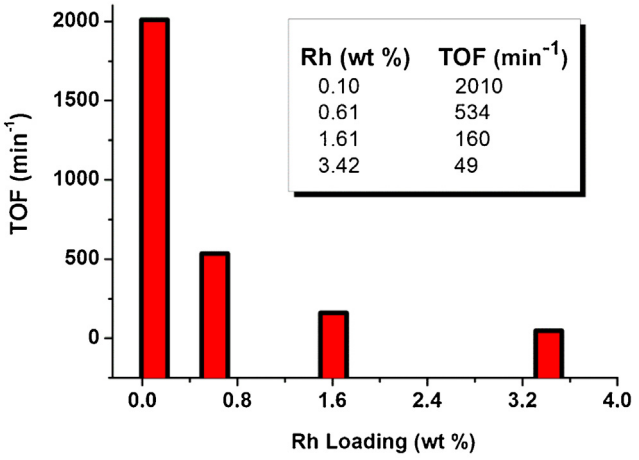

Fig. 6. The turnover frequency (TOF) values in hydrolysis of AB (100 mM) starting with Rh^0/CeO_2 (0.08 mM Rh) at different rhodium loading at 25.0 ± 0.1 °C.

2.4. Catalytic hydrolysis of AB using rhodium(0) nanoparticles supported on ceria

Before starting the hydrolysis of AB, a jacketed reaction flask (20 mL) containing a Teflon-coated stir bar was placed on a magnetic stirrer (Heidolph MR-301) and thermostated to 25.0 ± 0.1 °C by circulating water through its jacket from a constant temperature bath. Then, a graduated glass tube (60 cm in height and 3.0 cm in diameter) filled with water was connected to the reaction flask to measure the volume of the hydrogen gas to be evolved from the reaction. Next, 20 mg powder of Rh^0/CeO_2 was dispersed in 10 mL distilled water in the reaction flask thermostated at 25.0 ± 0.1 °C. Then, 31.8 mg AB (1.0 mmol $H_3N{\cdot}BH_3$) was added into the flask and the reaction medium was stirred at 1200 rpm. The volume of hydrogen gas evolved was measured by recording the displacement of water level every 1 min at constant atmospheric pressure of 693 Torr. The catalytic activity of Rh^0/SiO_2, Rh^0/Al_2O_3, Rh^0/ZrO_2, Rh^0/TiO_2, and Rh^0/HfO_2 was also tested by following the same procedure as described above under the same conditions at the same rhodium concentration.

2.5. Determination of the most active rhodium loading for Rh^0/CeO_2 in the hydrolysis of AB

The catalytic activity of Rh^0/CeO_2 samples with various rhodium loadings in the range of 0.1–4.0% wt. was tested in hydrogen generation from the hydrolysis of ammonia borane starting with 0.08 mM Rh and 100 mM AB in 10 mL solution at 25.0 ± 0.1 °C. The highest catalytic activity was achieved by using 0.1% wt. rhodium loaded ceria. For all the tests reported hereafter, rhodium loading of 0.1% wt. was used unless otherwise stated.

2.6. Determination of activation energy for the hydrolysis of AB catalyzed by Rh^0/CeO_2

In a typical experiment, the hydrolysis reaction was performed starting with 10 mL of 100 mM (31.8 mg) AB solution and 20 mg Rh^0/CeO_2 (0.1% wt. Rh), [Rh] = 0.02 mM) at various temperatures (20, 25, 30, 35 °C) in order to obtain the activation energy. The rate constant for the hydrogen generation reaction was calculated from the slope of the linear part of each hydrogen evolution versus time plot at various temperatures. Activation energy for the hydrolysis of ammonia borane catalyzed by Rh^0/CeO_2 was obtained from the slope of Arrhenius plot.

2.7. Reusability of Rh^{00}/CeO_2 in the hydrolysis of AB

After the complete hydrolysis of AB started with 10 mL of 100 mM AB (31.8 mg H_3NBH_3), and 80 mg Rh^0/CeO_2 (0.1% wt. Rh, [Rh] = 0.08 mM) at 25.0 ± 0.1 °C, the catalyst was isolated as dark grey powder by centrifugation and dried under vacuum (10^{-3} Torr) at 60 °C after washing with 50 mL of water. The isolated samples of Rh^0/CeO_2 were weighed (Table 3) and redispersed in 10 mL solution of 100 mM AB for a subsequent run of hydrolysis at 25.0 ± 0.1 °C.

2.8. Durability of Rh^{00}/CeO_2 catalyst in the hydrolysis of AB

Recyclability test was started with 10 mL of 100 mM AB (31.8 mg H_3NBH_3), and 80 mg Rh^0/CeO_2 (0.1% wt. Rh, [Rh] = 0.08 mM) at 25.0 ± 0.1 °C. When the AB present in the solution was completely hydrolyzed, 1 mmol AB was added for another run of hydrolysis.

3. Results and discussion

A series of survey experiments were performed to find out the best support for the rhodium(0) nanoparticles which would provide the highest catalytic activity in hydrogen generation from the hydrolysis of ammonia borane at room temperature. First, rhodium(III) ions were impregnated from the aqueous solution of rhodium(III) chloride on one of the following supports with the average particle size given in parentheses: CeO_2 (25 nm), SiO_2 (12 nm), Al_2O_3 (13 nm), TiO_2 (25 nm), ZrO_2 (100 nm), and HfO_2 (100 nm). Then, the impregnated rhodium(III) ions were reduced by sodium borohydride at room temperature yielding Rh^{00}/CeO_2, Rh^{00}/SiO_2, Rh^{00}/Al_2O_3, Rh^{00}/TiO_2, Rh^{00}/ZrO_2, and Rh^{00}/HfO_2, respectively. The metal content of the isolated powders was determined by ICP and given in Table 1.

The supported rhodium(0) nanoparticles were tested for their catalytic activity in hydrogen generation from the hydrolysis of ammonia borane. The catalytic hydrolysis of ammonia borane was followed by monitoring the change in H_2 volume, which was then converted into the equivalent H_2 per mole of AB using the known 3:1 H_2/AB stoichiometry (Eq. (1)). Fig. S1a and b shows the volume of hydrogen versus time plots for the hydrolysis of 0.10 M ammonia borane solution performed starting with rhodium(0) nanoparticles supported on different oxide nanopowders at high

Table 1
The rhodium contents and turnover frequency values of rhodium(0) nanoparticles supported on different oxide nanopowders at (a) high and (b) low rhodium loading of the catalysts used in hydrogen generation from the hydrolysis of ammonia borane at 25.0 ± 0.1 °C for a fair comparison.

Catalyst	Rh loading (%wt.)[a]	[Rh] conc. (mM)[a]	TOF (min^{-1})[a]	Rh loading (wt.%)[b]	[Rh] conc. (mM)[b]	TOF(min^{-1})[b]
Rh^0/CeO_2	1.61	0.08	161	0.10	0.08	2010
Rh^0/SiO_2	2.03	0.08	43	0.40	0.08	112
Rh^0/Al_2O_3	2.07	0.08	101	0.50	0.08	195
Rh^0/TiO_2	1.95	0.08	73	0.47	0.08	105
Rh^0/ZrO_2	2.12	0.08	15	0.59	0.08	102
Rh^0/HfO_2	1.92	0.08	29	0.48	0.08	24

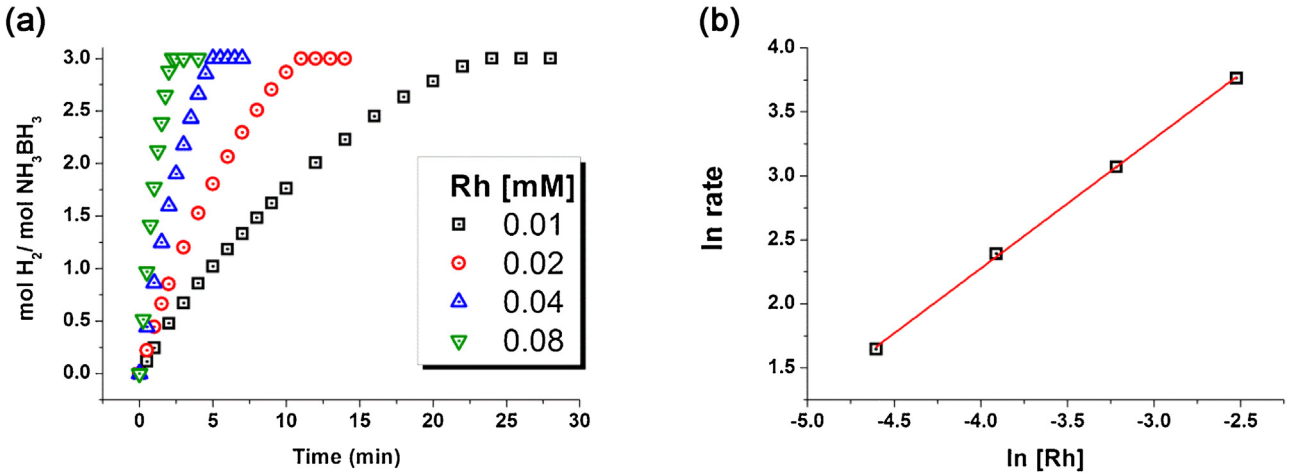

Fig. 7. (a) mol H_2/mol $H_3N{\cdot}BH_3$ versus time graph depending on the rhodium concentration in Rh^0/CeO_2 for the hydrolysis of AB (100 mM) at 25.0 ± 0.1 °C. (b) The logarithmic plot of hydrogen generation rate versus the concentration of Rh; ln (rate) = 1.01 ln [Rh] + 6.33.

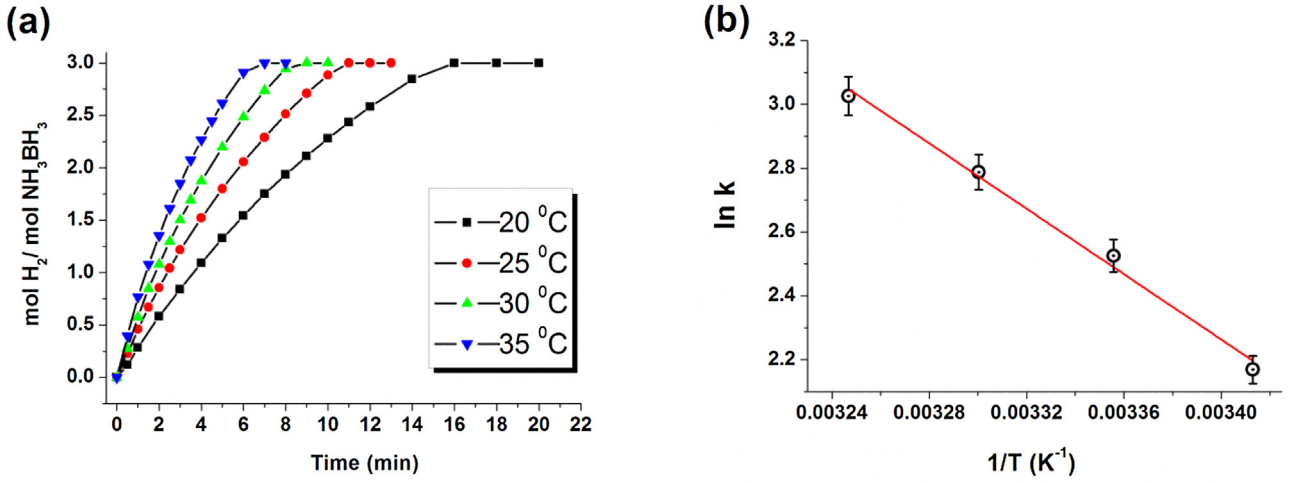

Fig. 8. (a) The evolution of equivalent hydrogen per mole of AB versus time plot for the hydrolysis of AB starting with Rh^0/CeO_2 (0.02 mM Rh) and 100 mM AB at various temperatures. (b) The Arrhenius plot for the Rh^0/CeO_2 catalyzed hydrolysis of AB. lnk = −5122.6(1/T) + 19.68.

and low rhodium loadings, respectively, at 25.0 ± 0.1 °C. The initial turnover frequency values were calculated from the initial rate of hydrogen generation and listed in Table 1. As it can easily be seen from the graphical illustration in Fig. 1, among the catalysts tested, rhodium(0) nanoparticles supported on nanoceria show the highest catalytic activity in hydrogen generation from the hydrolysis of ammonia borane at room temperature. Therefore, we decided to use nanoceria as support for the further investigation on rhodium(0) nanoparticles catalysts in hydrogen generation from the hydrolysis of ammonia borane.

Rhodium(0) nanoparticles supported on nanoceria (Rh^0/CeO_2) were isolated from the reaction solution by centrifugation, copious washing with water, and drying under vacuum (10^{-3} Torr) at 60 °C and characterized by ICP-OES, XRD, BET, SEM, SEM-EDS, TEM and XPS. Fig. 2 shows the XRD pattern of ceria powders and rhodium(0) nanoparticles supported on ceria (Rh^{00}/CeO_2) with two different rhodium loadings. Powder XRD pattern of Rh^0/CeO_2 in Fig. 2b exhibits peaks at 28.5°, 33.07°, 47.08°, 56.33° and 59.08° assigned to the (111), (200), (220), (311) and (222) reflections of CeO_2, respectively (JPDS = 43-1002). Comparison of the XRD patterns clearly shows that there is no change in intensity and position of the characteristic diffraction peaks of ceria. This observation indicates that ceria remains intact after reduction of rhodium(III) ions and there is no noticeable alteration in the framework lattice or

Table 2
Turnover frequency value (TOF) and activation energy (E_a) of the most active rhodium, ruthenium, palladium and platinum catalysts reported for the hydrolysis of AB at 25.0 ± 0.1 °C.

Catalyst	TOF (min^{-1})	E_a (kJ/mol)	Metal/AB molar ratio	Ref.
Rh^0/CeO_2 (0.1% wt. Rh)	2010	42.6	0.0008	This study
Rh(0)/CNT	706	32	0.0025	[15]
Pt/CNTs-O-HT	468	–	0.0047	[42]
Ru/CB	429.5	34.81	0.00425	[43]
Pt@MIL-101	414	40.7	0.0029	[44]
Pd@Co/graphene	408.9	–	0.02	[45]
Ru@MWCNT	329	33	0.00189	[46]
Rh/graphene	325	19.7	0.004	[38]
$Pt/\gamma\text{-}Al_2O_3$	308	21	0.018	[47]
$Rh(0)@TiO_2$	260	65.5	0.00116	[48]
$Pd(0)/SiO_2\text{-}CoFe_2O_4$	254	52	0.0031	[49]
Laurate stabilized Rh(0) nanocluster	200	43.6	0.0025	[50]
$Rh^0/nanoAl_2O_3$ (0.5% wt. Rh)	195	–	0.0008	This study
Pt/CeO_2	182	–	0.0018	[32]
$Ru(0)/SiO_2\text{-}CoFe_2O_4$	172.5	45.6	0.00097	[51]
Ru/HAp	137	58	0.00392	[52]
Ru/X-NW	135	77	0.00271	[53]
$Rh/\gamma\text{-}Al_2O_3$	128.2	21	0.018	[47]
$Rh^0/nanoSiO_2$ (0.4 wt.% Rh)	112	–	0.0008	This study
$Rh^0/nanoTiO_2$ (0.47% wt. Rh)	105	–	0.0008	This study
$Rh^0/nanoZrO_2$ (0.59% wt. Rh)	102	–	0.0008	This study
Zeolite stabilized Rh(0) nanocluster	92	66.9	0.002	[54]
Rh^0/HfO_2 (0.48% wt. Rh)	24	–	0.0008	This study

loss in the crystallinity of host material. There is no observable peak attributable to rhodium nanoparticles in Fig. 2, most likely as a result of low rhodium loading on ceria.

The BET nitrogen adsorption analysis (Fig. S2 in the Supporting information) gave the surface area of ceria and Rh^0/CeO_2 as 48.1 and 47.32 $m^2\ g^{-1}$, respectively. This slight decrease in the surface area of ceria upon rhodium loading implies the existence of rhodium(0) nanoparticles on the surface of support.

Fig. 3 exhibits the SEM image and SEM-EDS spectrum of Rh^0/CeO_2 indicating that rhodium is the only element detected in the sample in addition to the framework elements of ceria (Ce, O).

The morphology and size of rhodium nanoparticles on the surface of ceria were investigated by high resolution TEM (Fig. 4a–d) which shows rhodium nanoparticles with particle size in the range 1.8–5.3 nm (average diameter: 3.2 ± 0.8 nm, histogram in Fig. 4e) are successfully anchored on ceria nanopowder.

The composition of Rh^0/CeO_2 and the oxidation state of rhodium were also studied by XPS technique. The survey-scan XPS spectrum of Rh^0/CeO_2 with a rhodium loading of 0.1% wt. given in Fig. 5 shows the presence of all the framework elements of Rh^0/CeO_2 in agreement with the SEM-EDS result. High resolution X-ray photoelectron spectrum of Rh^0/CeO_2 sample given in the inset of Fig. 5 shows two prominent Rh 3d bands at 307.07 eV and 312.10 eV which can readily be assigned to Rh(0) $3d_{5/2}$ and $3d_{3/2}$ bands, respectively, by comparing to the values of metallic rhodium [38]. The bands at 309.8 and 305.2 eV (inset of Fig. 5) are attributable to rhodium oxide [39], which might be formed during the XPS sampling. For comparison, high resolution XPS spectra of CeO_2 and Rh^{00}/CeO_2 with a rhodium loading of 0.1% wt. in Ce 3d and Ce 4d regions are given in Fig. S3 of the Supporting Information. There is no observable change in the spectra after rhodium loading.

Before starting with the investigation on the catalytic activity of Rh^0/CeO_2 in the hydrolysis of ammonia borane, a control experiment was performed to check whether ceria shows any catalytic activity in the hydrolysis of ammonia borane at the same temperature. In the control experiments performed starting with 1.0 mmol AB and 80 mg CeO_2 (the same amount as the one used in catalytic activity tests) in 10 mL of water at 20.0 or 35.0 ± 0.1 °C, no hydrogen generation was observed in 1 h at both temperatures. This observation indicates that the hydrolysis of ammonia borane does not occur in the presence of CeO_2 in the temperature range used in this study. However, Rh^0/CeO_2 is found to be highly active catalyst in the hydrolysis of ammonia borane generating 3.0 equivalent H_2 gas per mole of AB in the same temperature range. AB molecule interacts with the active site of the metal particle and an activated complex is formed. Then, B—N bond dissociation takes place by the attack of water molecule on the activated complex, which results in the hydrolysis of the BH_3 intermediate to form the borate ion together with the release of H_2 [40,41].

Table 3
The TOF value of Rh^0/CeO_2 (0.1% wt. Rh) in the subsequent runs of the hydrolysis of ammonia borane (The material loss has been taken into account for the TOF calculations in each run).

Run	Rh^0/CeO_2 (mg)	[Rh] (mM)	TOF (min^{-1})
1	80	0.080	2010
2	72	0.072	1540
3	64	0.064	1470
4	61	0.061	1450
5	56	0.056	1350

The catalytic activity of Rh^0/CeO_2 in hydrogen generation from the hydrolysis of ammonia borane at 25.0 ± 0.1 °C was investigated depending on the rhodium loading of catalyst. The plots of equivalent H_2 gas generated per mole of H_3NBH_3 versus time during the catalytic hydrolysis of 100 mM AB solution using Rh^0/CeO_2 with different loading at 25.0 ± 0.1 °C are available in Fig. S4 of the Supporting Information. The turnover frequency (TOF) values were calculated from the initial rate measured in each of the hydrogen generation versus time plots given in Fig. S4 of the Supporting Information. The variation of TOF with the rhodium loading of the catalyst is illustrated in Fig. 6. It is seen that the Rh^0/CeO_2 sample with a rhodium loading of 0.1% wt. Rh provides the highest catalytic activity in hydrogen generation from the hydrolysis of ammonia borane at 25.0 ± 0.1 °C. Therefore, Rh^0/CeO_2 catalyst with rhodium loading of 0.1% wt. Rh was used in all of the further experiments performed in this study. The decrease in catalytic activity of Rh^0/CeO_2 with the increasing rhodium loading may be attributed to the aggregation of rhodium nanoparticles as seen from the TEM images in Fig. S5.

Fig. 7a shows the plots of equivalent H_2 gas generated per mole of H_3NBH_3 versus time during the catalytic hydrolysis of 100 mM AB solution using Rh^0/CeO_2 catalyst in different rhodium

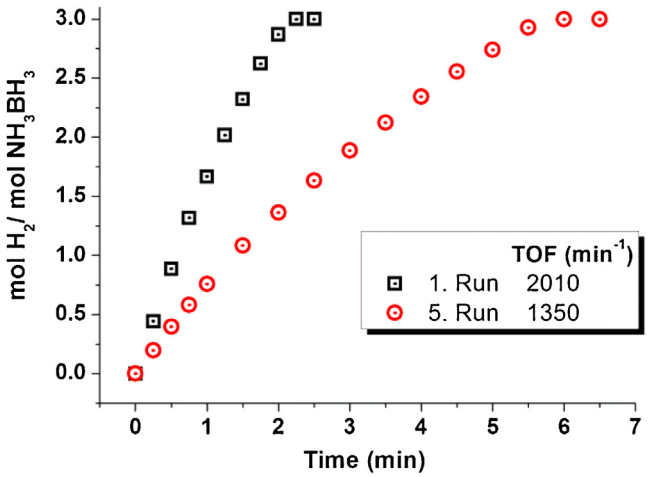

Fig. 9. Graph of the evolution of equivalent hydrogen per mole of AB versus time plot for the first and fifth use of Rh^0/CeO_2 (0.1% wt. Rh) in catalytic hydrolysis of AB for at 25.0 ± 0.1 °C.

concentration at 25.0 ± 0.1 °C. The hydrogen generation rate was determined from the linear portion of each plot in Fig. 7a and plotted versus the initial concentration of rhodium, both in logarithmic scale, in Fig. 7b, which gives straight line with a slope of 1.01 indicating that the catalytic hydrolysis of ammonia borane is first order with respect to the rhodium concentration.

The TOF values for hydrogen generation from the hydrolysis of ammonia borane (100 mM) at 25.0 ± 0.1 °C were determined from the hydrogen generation rate in the linear portion of the plots given in Fig. 7a for experiment performed starting with 100 mM AB plus Rh^0/CeO_2 (0.1% wt. Rh) in various rhodium concentrations. The TOF value of Rh^0/CeO_2 catalyst in rhodium concentration of 0.08 mM Rh is as high as 2010 min^{-1} in hydrogen generation from the hydrolysis of ammonia borane at 25.0 ± 0.1 °C. TOF values of the most active rhodium, platinum, ruthenium catalysts used in hydrogen generation from the hydrolysis of ammonia borane are listed in Table 2 for comparison. As clearly seen from the TOF values listed in Table 2, rhodium(0) nanoparticles supported on nanoceria (Rh^0/CeO_2) provide the highest catalytic activity (TOF = 2010 min^{-1}) ever reported for the room temperature hydrolysis of ammonia borane in literature. This high catalytic activity of Rh^0/CeO_2 can be attributed to the fact that ceria is a reducible oxide support [20]. Because of large standard reduction potential of $Ce^{4+} \rightarrow Ce^{3+}$ (1.76 V in acidic solution) [21], Ce^{3+} defects can easily be formed in ceria under the reaction conditions leading to the build up of excess negative charge on the oxide surface. This negative charge on the oxide surface can bind the rhodium(0) nanoparticles strongly making the surface rhodium sites catalytically more active in hydrogen generation from the hydrolysis of ammonia borane.

Catalytic hydrolysis of ammonia borane was also performed starting with 100 mM AB in the presence of Rh^0/CeO_2 (0.02 mM Rh) at various temperatures. Fig. 8a shows the evolution of equivalent H_2 per mole of ammonia borane versus time plots for the hydrolysis of AB at various temperatures in the range 20–35 °C. The rate constant for the hydrogen generation reactions was calculated from the slope of the linear part of each hydrogen evolution versus time plot at various temperatures (Fig. 8a). From the slope of Arrhenius plot in Fig. 8b, activation energy for the hydrolysis of ammonia borane catalyzed by Rh^0/CeO_2 was found to be E_a = 43 ± 2 kJ/mol, which is comparable to the literature values reported for the other catalysts used in the same reaction (Table 2).

Reusability of Rh^0/CeO_2 catalyst was tested in successive experiments performed using the catalyst isolated from the reaction solution after a previous run of hydrolysis of ammonia borane. After the completion of hydrogen generation from the hydrolysis of ammonia borane starting with 0.08 mM Rh^0/CeO_2 plus 100 mM AB in 10 mL aqueous solution at 25.0 ± 0.1 °C, the catalyst was isolated by centrifugation and dried under vacuum (10^{-3} torr) at 60 °C after washing with 50 mL of water. The isolated solid sample of Rh^0/CeO_2 was weighed and redispersed in 10 mL solution of 100 mM AB for a subsequent run of hydrolysis which was then started immediately and continued until the completion of hydrogen evolution at 25.0 ± 0.1 °C. This hydrogen generation process was repeated 5 times in the same way at 25.0 ± 0.1 °C and the results are listed in Table 3. The results of reusability tests reveal that Rh^0/CeO_2 are still active in the subsequent runs of hydrolysis of ammonia borane providing 100% conversion (yielding 3 equivalent H_2 per mole of AB).

Fig. 9 shows the evolution of equivalent H_2 per mole of H_3NBH_3 versus time plot for the first and fifth use of Rh^0/CeO_2 (0.08 mM Rh) in catalytic hydrolysis of ammonia borane at 25.0 ± 0.1 °C. After the fifth run of hydrolysis of ammonia borane, Rh^0/CeO_2 still exhibits a record TOF value (1350 min^{-1}), preserving 67% of the initial catalytic activity. The decrease in catalytic activity in successive runs (Table 3) can be attributed to the agglomeration of nanoparticles on the surface of ceria during the isolation, drying and redispersion processes. Indeed, the TEM image in Fig. 10a for the sample harvested after the fifth run of hydrolysis indicates the agglomeration of rhodium(0) nanoparticles on the surface of ceria.

Durability of the Rh^0/CeO_2 (0.1% wt. Rh) catalyst was also tested in hydrogen generation from the hydrolysis of ammonia borane. For the recyclability test, a standard hydrolysis of ammonia borane catalyzed by Rh^0/CeO_2 was performed starting with 10 mL solution of 100 mM AB and 0.08 mM Rh at 25.0 ± 0.1 °C. When the ammonia

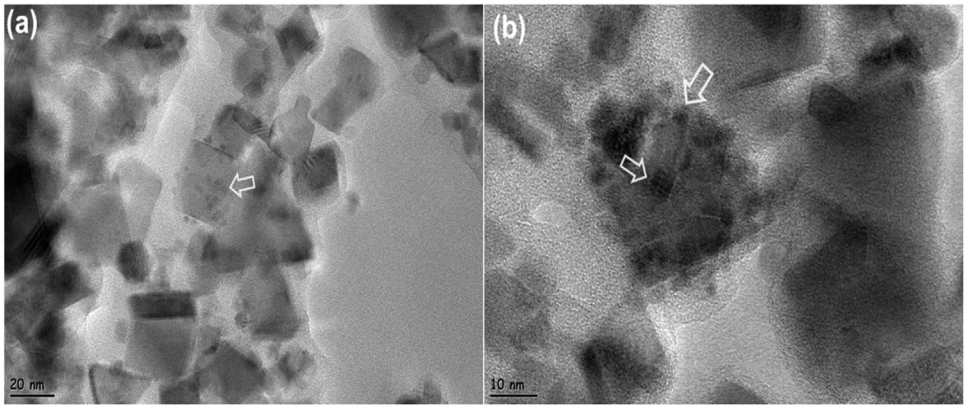

Fig. 10. TEM image of Rh^0/CeO_2 sample (0.1% wt. Rh) harvested after the fifth use (a) and fifth cycle (b) in hydrolysis of AB at 25.0 ± 0.1 °C.

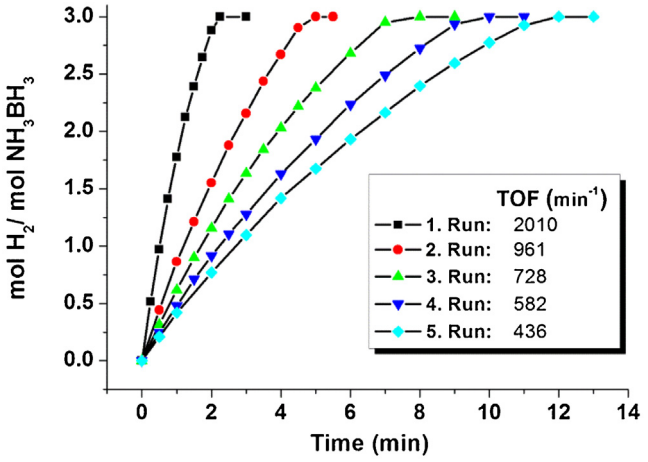

Fig. 11. Graph of the evolution of equivalent hydrogen per mole of AB versus time plot for the Rh^0/CeO_2 (0.08 mM Rh) catalytic hydrolysis of AB from 1st to 5th cycles at 25.0 ± 1.0 °C.

borane present in the solution was completely hydrolyzed, 1 mmol AB was added for the next run of hydrolysis. The results of 5 recyclability tests are given in Fig. 11 showing that Rh^0/CeO_2 catalysts are still active after multiple cycles of reaction providing the generation of 3 equivalent H_2 per mole of ammonia borane. However, the catalytic activity of Rh^0/CeO_2 decreases to some extent after each cycle. After five cycles, the Rh^0/CeO_2 catalysts retain only 22% of the initial catalytic activity in hydrogen generation from the hydrolysis of ammonia borane.

The catalytic activity of the filtrate solution obtained by centrifugation of the solid materials after the fifth cycle was also tested in the hydrolysis of ammonia borane (100 mM) under the same conditions. The filtrate solution is catalytically silent in hydrolysis of ammonia borane. Therefore, the deactivation of Rh^{00}/CeO_2 catalyst can be attributed to a decrease in accessibility of active sites of rhodium nanoparticles due to the passivation of metal surface by metaborate ions which accumulate in solution as the reaction proceeds. In addition, the decrease in catalytic activity in successive runs can also be attributed to the agglomeration of nanoparticles on the surface of ceria as shown in TEM image (Fig. 10b) taken after the fifth cycle.

4. Conclusion

In summary, the followings are the main results of the present study:

Rhodium(0) nanoparticles supported on nanoceria are prepared by the impregnation of Rh^{3+} ions on the surface of ceria followed by the sodium borohydride reduction of Rh^{3+} ions in aqueous solution at room temperature (Rh^0/CeO_2).

Rh^{00}/CeO_2 is highly active catalyst in hydrogen generation from the hydrolysis of ammonia borane providing the highest TOF value (2010 min^{-1}) at 25.0 ± 0.1 °C ever reported for this reaction in literature.

Rh^0/CeO_2 also shows the highest catalytic activity among the rhodium(0) nanoparticles supported on nanopowders of CeO_2, SiO_2, Al_2O_3, TiO_2, ZrO_2, and HfO_2 tested in the room temperature hydrolysis of ammonia borane under the same reaction conditions.

This superb catalytic activity of Rh^0/CeO_2 can be ascribed to the reducible nature of oxide support [21]. Because of large standard reduction potential of $Ce^{4+} \rightarrow Ce^{3+}$ (1.76 V in acidic solution) [22], Ce^{3+} defects can easily be formed in ceria under the reaction conditions leading to the build up of excess negative charge on the oxide surface. This negative charge on the oxide surface can bind the rhodium(0) nanoparticles strongly making the surface metal sites catalytically more active in hydrogen generation from the hydrolysis of ammonia borane.

Rh^0/CeO_2 are reusable catalyst preserving 67% of the initial catalytic activity, even after the fifth use in hydrogen generation from the hydrolysis of ammonia borane at room temperature. It is noteworthy that Rh^0/CeO_2 provide a record TOF value of 1350 min^{-1} even after the fifth use in hydrogen generation from the hydrolysis of ammonia borane at 25.0 ± 0.1 °C.

The facile preparation, superb catalytic activity and reusability make Rh^0/CeO_2 very attractive catalyst for hydrogen generation from the hydrolysis of ammonia borane which can be used as solid hydrogen storage materials in portable fuel cell applications.

This simple facile method developed for the preparation of rhodium(0) nanoparticles supported on ceria can be extended to other ceria-based metallic systems in other applications in the field of catalysis.

Acknowledgements

Partial support by Turkish Academy of Sciences (TUBA) is gratefully acknowledged. We would like to thank İlker Yıldız for XPS analyses.

Appendix A. Supplementary data

Supplementary data associated with this article can be found, in the online version, at http://dx.doi.org/10.1016/j.apcatb.2016.05.061.

References

[1] B. Peng, J. Chen, Energy Environ. Sci. 1 (2008) 479–483.
[2] U.B. Demirci, P. Miele, Energy Environ. Sci. 2 (2009) 627–637.
[3] N.C. Smythe, J.C. Gordon, Eur. J. Inorg. Chem. 4 (2010) 509–521.
[4] T. Umegaki, J.M. Yan, X.B. Zhang, H. Shioyama, N. Kuriyama, Q. Xu, Int. J. Hydrogen Energy 34 (2009) 2303–2311.
[5] F.H. Stephens, V. Pons, R.T. Baker, Dalton Trans. 25 (2007) 2613–2626.
[6] S.K. Kim, W.S. Han, T.J. Kim, T.Y. Kim, S.W. Nam, M. Mitoraj, L. Piekos, A. Michalak, S.J. Hwang, S.O. Kang, J. Am. Chem. Soc. 132 (2010) 9954–9955.
[7] Ö. Metin, S. Sahin, S. Özkar, Int. J. Hydrogen Energy 630 (2009) 6304–6313.
[8] H.Y. Liang, G.Z. Chen, S. Desinan, R. Rosei, F. Rosei, D.L. Ma, Int. J. Hydrogen Energy 37 (2012) 17921–17927.
[9] S. Akbayrak, S. Tanyıldızı, İ. Morkan, S. Özkar, Int. J. Hydrogen Energy 39 (2014) 9628–9637.
[10] L.T. Guo, Y.Y. Cai, J.M. Ge, Y.N. Zhang, L.H. Gong, X.H. Li, K.X. Wang, Q.Z. Ren, J. Su, J.S. Chen, (2015) 388–392.
[11] Ö. Metin, V. Mazumder, S. Özkar, S. Sun, J. Am. Chem. Soc. 132 (2010) 1468–1469.
[12] M. Dinç, Ö. Metin, S. Özkar, Catal. Today 183 (2012) 10–16.
[13] Q. Yao, Z.-H. Lu, Y. Wang, X. Chen, G. Feng, J. Phys. Chem. C 119 (2015) 14167–14174.
[14] Q. Yao, Z.-H. Lu, Z. Zhang, X. Chen, Y. Lan, Sci. Rep. 4 (2014) 7597–8005.
[15] D.W. Himmelberger, C.W. Yoon, M.E. Bluhm, P.J. Carroll, L.G. Sneddon, J. Am. Chem. Soc. 131 (2009) 14101–14110.
[16] Q. Yao, Z.H. Lu, Y. Jia, X. Chen, X. Liu, Int. J. Hydrogen Energy 40 (2015) 2207–2215.
[17] Y. Lin, R.G. Finke, J. Am. Chem. Soc. 116 (1994) 8335–8353.
[18] Y. Wan, H.Y. Wang, Q.F. Zhao, M. Klingstedt, O. Terasaki, D.Y. Zhao, J. Am. Chem. Soc. 131 (2009) 4541–4550.
[19] L. Yang, W. Luo, G.Z. Cheng, ACS Appl. Mater. Interfaces 5 (2013) 8231–8240.
[20] Q.L. Zhu, J. Li, Q. Xu, J. Am. Chem. Soc. 135 (2013) 10210–10213.
[21] A. Ciftci, S. Eren, D.A.J.M. Ligthart, E.J.M. Hensen, Chem. Cat. Chem. 6 (2014) 1260–1269.
[22] A.J. Bard, R. Parsons, J. Jordan, Standard Potentials in Aqueous Solution, IUPAC, Marcel Dekker Inc., New York, New York, 1985.
[23] S.S. Lee, W. Song, M. Cho, H.L. Puppala, P. Nguyen, H. Zhu, L. Segatori, V.L. Colvin, ACS Nano 7 (2013) 9693–9703.
[24] L. He, B. Liang, L. Li, X. Yang, Y. Huang, A. Wang, X. Wang, T. Zhang, ACS Catalysis 5 (2015) 1623–1628.
[25] M. Cargnello, V. Doan-Nguyen, T. Gordon, R. Diaz, E. Stach, R. Gorte, P. Fornasiero, C. Murray, Science 341 (2013) 771–773.
[26] C. Sun, H. Li, L. Chen, Energy Environ. Sci. 5 (2012) 8475–8505.
[27] Z. Zhang, Z.-H. Lu, H. Tan, X. Chen, Q. Yao, J. Mater. Chem. A 3 (2015) 23520–23529.
[28] S.P.S. Badwal, D. Fini, F.T. Ciacchi, C. Munnings, J.A. Kimpton, J. Drennan, J. Mater. Chem. A 1 (2013) 10768–10782.

[29] A. Le Gal, S. Abanades, N. Bion, T. Le Mercier, V. Harle, Energy Fuels 27 (2013) 6068–6078.
[30] N. Ta, J. Liu, S. Chenna, P. Crozier, Y. Li, A. Chen, W. Shen, J. Am. Chem. Soc. 134 (2012) 20585–20588.
[31] A. Bruix, J. Rodriguez, P. Ramírez, S. Senanayake, J. Evans, J. Park, D. Stacchiola, P. Liu, J. Hrbek, F. Illas, J. Am. Chem. Soc. 134 (2012) 8968–8974.
[32] X. Wang, D.P. Liu, S.Y. Song, H.J. Zhang, Chem. Commun. 48 (2012) 10207–10209.
[33] L. He, B. Liang, L. Lin, X. Yang, Y. Huang, A. Wang, X. Wang, T. Zhang, ACS Catalysis 5 (2015) 1623–1628.
[34] J. Graciani, K. Mudiyanselage, F. Xu, A.E. Baber, J. Evans, S.D. Senanayake, D.J. Stacchiola, P. Liu, J. Hrbek, J. Fernandez Sanz, J.A. Rodriguez, Science 345 (2014) 546–550.
[35] C. Tang, H. Zhang, L. Dong, Catal. Sci. Technol. 6 (2016) 1248–1264.
[36] B. Goris, S. Turner, S. Bals, G.V. Tendeloo, ACS Nano 8 (2014) 10878–10884.
[37] A. Rehman, S. Hossain, S. Rahman, S. Ahmed, M.M. Hossain, Electrocatalytic 6 (2015) 348–356.
[38] J. Shen, L. Yang, K. Hu, W. Luo, G. Cheng, Int. J. Hydrogen Energy 40 (2015) 1062–1070.
[39] G. Gallaher, J.G. Goodwin, C.S. Huang, M. Houalla, J. Catal. 127 (1991) 719–731.
[40] M. Chandra, Q. Xu, J. Power Sources 159 (2006) 855–860.
[41] M. Mahyari, A. Shaabani, J. Mater. Chem. A 2 (2014) 16652–16659.
[42] W. Chen, J. Ji, X. Duan, G. Qian, P. Li, X. Zhou, D. Chen, W. Yuan, Chem. Commun 50 (2014) 2142–2144.
[43] H. Liang, G. Chen, S. Desinan, R. Rosei, F. Rosei, D. Ma, Int. J. Hydrogen Energy 3 (2012) 17921–17927.
[44] A. Aijaz, A. Karkamkar, Y.J. Choi, N. Tsumori, E. Rönnebro, T. Autrey, H. Shioyama, Q. Xu, J. Am. Chem. Soc. 134 (2012) 13926–13929.
[45] J. Wang, Y.L. Qin, X. Liu, X.B. Zhang, J. Mater. Chem. 22 (2012) 12468–12470.
[46] S. Akbayrak, S. Özkar, ACS Appl Mater. Interfaces 4 (2012) 6302–6310.
[47] M. Chandra, Q. Xu, J. Power Sources 168 (2007) 135–142.
[48] S. Akbayrak, S. Gençtürk, İ. Morkan, S. Özkar, RCS Advances 4 (2014) 13742–13748.
[49] S. Akbayrak, M. Kaya, M. Volkan, S. Özkar, Appl. Catal. B 147 (2014) 387–393.
[50] F. Durap, M. Zahmakıran, S. Özkar, Appl. Catal. A 369 (2009) 53–59.
[51] S. Akbayrak, M. Kaya, M. Volkan, S. Özkar, J. Mol. Catal. A 394 (2014) 253–261.
[52] S. Akbayrak, P. Erdek, S. Özkar, Appl. Catal. B 142–143 (2013) 187–195.
[53] S. Akbayrak, S. Özkar, Dalton Trans. 43 (2014) 1797–1805.
[54] M. Zahmakıran, S. Özkar, Appl. Catal. B 89 (2009) 104–110.